HHS Public Access

Author manuscript

Oncogene. Author manuscript; available in PMC 2022 March 01.

Published in final edited form as:

Oncogene. 2021 August ; 40(33): 5182–5191. doi:10.1038/s41388-021-01919-x.

Targeting HIF-activated collagen prolyl 4-hydroxylase expression disrupts collagen deposition and blocks primary and metastatic uveal melanoma growth

Stefan Kaluz[1,2,12], **Qing Zhang**[3,4,12], **Yuki Kuranaga**[5], **Hua Yang**[3], **Satoru Osuka**[1,5,6], **Debanjan Bhattacharya**[1], **Narra S. Devi**[1], **Jiyoung Mun**[7], **Wei Wang**[8,9], **Ruiwen Zhang**[8,9], **Mark M. Goodman**[2,7], **Hans E. Grossniklaus**[2,3,10,✉], **Erwin G. Van Meir**[1,2,5,6,11,✉]

[1]Department of Neurosurgery, Emory University, Atlanta, GA, USA

[2]Winship Cancer Institute, Emory University, Atlanta, GA, USA

[3]Department of Ophthalmology, Emory University, Atlanta, GA, USA

[4]Department of Ophthalmology, the Second Xiangya Hospital, Central South University, Changsha, Hunan, China

[5]Department of Neurosurgery, University of Alabama at Birmingham, Birmingham, AL, USA

[6]O'Neal Comprehensive Cancer Center, University of Alabama at Birmingham, Birmingham, AL, USA

[7]Department of Radiology and Imaging Sciences, Emory University, Atlanta, GA, USA

[8]Department of Pharmacological and Pharmaceutical Sciences, University of Houston, Houston, TX, USA

[9]Drug Discovery Institute, College of Pharmacy, University of Houston, Houston, TX, USA

[10]Department of Pathology, Emory University, Atlanta, GA, USA

[11]Department of Hematology and Medical Oncology, Emory University, Atlanta, GA, USA

Abstract

Uveal melanoma (UM) is the most prevalent primary intraocular malignancy in adults, and patients that develop metastases (~50%) survive <1 year, highlighting the urgent need for new therapies. TCGA has recently revealed that a hypoxia gene signature is associated with poor UM patient prognosis. Here we show that expression of hypoxia-regulated collagen prolyl-4-hydroxylase genes *P4HA1* and *P4HA2* is significantly upregulated in UM patients with metastatic disease and correlates with poor prognosis, suggesting these enzymes might be

✉**Correspondence** and requests for materials should be addressed to H.E.G. or E.G.V.M. ophtheg@emory.edu; evanmeir@uab.edu.
[12]These authors contributed equally: Stefan Kaluz, Qing Zhang.

COMPETING INTERESTS

EGVM is an inventor on a patent jointly held by Emory University and Scripps Research Institute that includes the KCN1 compound used in this study. He is also a share-holder of OncoSpherix Inc.

Supplementary information The online version contains supplementary material available at https://doi.org/10.1038/s41388-021-01919-x.

key tumor drivers. We targeted hypoxia-induced expression of P4HA1/2 in UM with KCN1, a hypoxia inducible factor-1 (HIF-1) pathway inhibitor and found potent inhibition of primary and metastatic disease and extension of animal survival, without overt side effects. At the molecular level, KCN1 antagonized hypoxia-induced expression of P4HA1 and P4HA2, which regulate collagen maturation and deposition in the extracellular matrix. The treatment decreased prolyl hydroxylation, induced proteolytic cleavage and rendered a disordered structure to collagen VI, the main collagen produced by UM, and reduced UM cell invasion. Together, these data demonstrate that extracellular collagen matrix formation can be targeted in UM by inhibiting hypoxia-induced P4HA1 and P4HA2 expression, warranting further development of this strategy in patients with uveal melanoma.

INTRODUCTION

Uveal melanoma (UM) is the most prevalent primary intraocular malignancy in adults [1, 2]. The overall mortality rate of UM patients is at 50% at 5 years and has remained unchanged for the last 40 years [1, 3, 4]. Enucleation or plaque radiotherapy can control the primary eye tumor; however, ~50% of patients develop metastases after which the mean survival time drops to <1 year. This progression is the rate-limiting step associated with a ~100% mortality and new therapies are urgently needed [5].

Metastasis, a complex and dynamic process in which highly aggressive tumor cells disseminate from their tissue of origin, associates with high patient mortality [6, 7]. The propensity of tumors to metastasize is influenced by the microenvironment in both the primary tumor and the target tissue [8]. Hypoxia, a reduction in partial oxygen pressure in the tumor tissue microenvironment, activates the hypoxia-inducible factor (HIF) transcription program, which leads to the production of a large number of gene products that play a critical role in each step of the metastatic process: migration/invasion; intra- /extravasation; preparation of the pre-metastatic niche; and facilitation of distant organ growth [9]. Integrated molecular characterization of UM through the TCGA has revealed a hypoxia gene signature characterizes one of the poor prognosis groups with high metastatic rate [10]. Prior studies in UM have shown that HIF promotes tumor progression by regulating proliferation, migration, invasion, and adhesion [11, 12] of tumor cells as well as angiogenesis [13, 14]. However, the role of HIF in directing pro-invasive extracellular matrix (ECM) remodeling has not been extensively investigated in UM.

Changes in ECM, including localized increases in collagen deposition and reorganization of collagen fibers, facilitate cancer progression and invasion of tumor cells [15]. Collagen maturation is a complex process that requires multiple intra- and extracellular posttranslational modifications [16]. Proline hydroxylation of procollagen polypeptide chains, catalyzed by collagen prolyl 4-hydroxylases (P4H) in the endoplasmic reticulum, is required for folding into helical structures and subsequent extracellular secretion [16]. Hypoxia promotes collagen deposition in part due to transcriptional activation of *P4HA1* and *P4HA2* (coding for A subunits of the tetrameric P4H) genes by HIF [17, 18].

The objective of this study was to evaluate the expression of collagen P4H genes in relation to UM patient prognosis, and to determine whether inhibiting hypoxia-induced P4HA1/2 expression in preclinical models of metastatic UM would lead to a therapeutic benefit.

RESULTS

Interrogation of hypoxia-induced pro-invasive/metastatic signaling genes in uveal melanoma patients reveals association of collagen maturation genes with survival

Hypoxia/HIF activates expression of over 50 known metastasis-promoting genes [9]. To gain an insight as to which ones might be important in UM development, we first examined their expression in a panel of human UM cell lines representative of the heterogeneity of the disease. qRT-PCR showed that only a subset is consistently expressed and activated by hypoxia (Fig. 1A and Supplementary Fig. 1A, B). To identify the most clinically-relevant, we probed their expression in datasets from UM patients with and without metastatic disease and only few genes showed potential correlation (Fig. 1B and Supplementary Fig. 1C). Bioinformatics analyses revealed that *P4HA1/2* ($p < 0.001$;Fig. 1C, left), and to a lesser extent *HK1/2, PGF, PLOD1* and *SLC2A3* ($p < 0.05$;Supplementary Fig. 2) are significantly overexpressed in patients with metastatic disease. Among these, only *P4HA1/2* expression correlates with poor overall survival in UM patients (Fig. 1C, right and Supplementary Fig. 3). These results suggest that P4HA1 and 2 can serve as prognostic markers in UM and may be important for malignant progression and patient survival.

Small molecule HIF transcription factor inhibitor blocks hypoxia-induced expression of *P4HA1/2* genes in UM melanoma cells

P4HA1/2 are important enzymes needed for collagen maturation and secretion, a prerequisite for tumor invasion/metastasis [19], suggesting that their targeting might be effective in UM metastasis. Therefore, we sought to target hypoxia-induced expression of P4HA1/2 in UM with a small molecule HIF pathway inhibitor. To guide the selection of HIF inhibitor, we probed for small molecules that had favorable distribution in the eye and liver and focused on KCN1, an arylsulfonamide that inhibits HIF transcription through a mechanism involving the block of HIF-1α association with co-factors p300 and CBP [20–24].

Initial pharmacokinetic studies with systemic delivery of unlabeled KCN1 suggested favorable distribution in the eye and liver (Supplementary Fig. 4A). To confirm, we performed a microPET experiment with radiolabeled KCN1. We synthesized [^{11}C]KCN1, injected it in the circulation and it reached a quasiequilibrium in organ biodistribution 5 min post-injection (Supplementary Fig. 4B,C). The time activity curves of drug distribution show that [^{11}C]KCN1 is abundantly up taken in liver and eyes, to levels 2–3 times higher than in brain (Supplementary Fig. 4D). The radio-ligand is also abundant in the gastrointestinal system. These data suggested that KCN1 is particularly well-suited for the treatment of ocular melanoma and its liver metastases.

We then examined whether KCN1 could inhibit expression of hypoxia-induced invasion/metastasis-related genes in the above UM cell lines. The genes most consistently

upregulated by hypoxia and inhibited by KCN1 in all cell lines (Fig. 1A, E right panel, Supplementary Fig. 1 and Supplementary Table 3A, B) were those coding for P4HA1 and 2 and procollagen-lysine 5-dioxygenase 1 and 2 (PLOD1 and 2), all involved in collagen synthesis. Validation of these findings at the protein level confirmed hypoxia induced the expression of P4HA1 and 2 enzymes in all five human UM cell lines and mouse melanoma cell line tested, and this was reduced by KCN1 (Fig. 1E left panel and Supplementary Fig. 1E, F). As KCN1 suppresses the protein expression of HIF-1α and HIF-2α, we further assessed whether hypoxia induction of P4HA1 and 2 expression through hypoxia responsive elements in their genes (Supplementary Fig. 1D) involved HIF-1 or HIF-2. We treated the cells with siRNAs targeting HIF-1α or HIF-2α and found that their induction was mostly dependent upon HIF-1 (Fig. 1E and Supplementary Fig. 1F).

These data confirm that P4HA1/2 are induced by hypoxia/HIF-1 in UM and that this response can be blunted by KCN1, a small molecule HIF inhibitor that distributes efficiently to eye and liver.

Dose- and time-dependent antitumor effects of KCN1 in an orthotopic immunocompetent mouse eye melanoma model

We next examined whether KCN1-mediated inhibition of the hypoxia response would have antitumor effects in UM mouse models. We initially tested antitumor potency and optimal dose and dosage regimen, in a syngeneic mouse model (Fig. 2). Melanoma cells (B16LS9) were inoculated in the uveal layer of the eye of syngeneic C57BL/6 mice, and mice were treated with single or twice daily i.p. doses of 30 or 60 mg/kg KCN1. On day 7 the eyes with tumors were enucleated, fixed and sectioned, and the effect of KCN1 was estimated by measuring tumor size as average largest surface occupied by the tumor. Results indicate that the higher single dose has stronger antitumor effect ($p < 0.01$). Delivering KCN1 twice daily at 30 mg/kg is equivalent to the single 60 mg/kg dose, whereas there is little added therapeutic benefit in the eye when delivering 60 mg/kg twice per day (Fig. 2A). To determine the importance of time to treatment, administration started on either day 1, 4 or 7 after intraocular implantation and the mouse eyes were evaluated for tumor size at day 7. Intraocular tumors were smaller in the group where the treatment was started on the 1st day versus the 4th or 7th days ($p < 0.05$) (Fig. 2B). These data demonstrate the strong antitumor effect of systemic treatment with KCN1 in the eye, establish a maximally effective dose of 60 mg/kg per day, and show the importance of early treatment.

To further examine KCN1's impact on the formation of distant liver metastases in the B16LS9 model, we counted the number of hepatic metastatic foci in liver sections (Fig. 2C). There was more than 50% reduction in the number of micro-metastases following treatment with the highest tested dose of KCN1, injected either once or twice daily compared with the control group ($p < 0.05$) (Fig. 2C, bottom).

Part of the inhibition of liver metastases formation is imparted by the antitumor effect at the primary tumor site as there were significantly fewer hepatic micro-metastases in mice that started their treatment on the 1st day post-implantation (~54% reduction), versus the 7th day after removal of the eye tumor (~26% reduction). These figures show that ~50% of the antimetastatic efficacy of KCN1 is retained when the treatment starts on day 7, and reflects

its impact on events downstream of tumor cell intravasation (Fig. 2D, top). In a longitudinal experiment, we observed a doubling in the number of micro-metastatic foci every 2 weeks and this was significantly lowered by ~50% in mice treated with KCN1 compared to vehicle controls at 1, 2, 3 and 4 weeks after tumor cell inoculation ($p < 0.05$) (Fig. 2D, bottom).

To further determine whether KCN1 also inhibits progression from micro- to macro-metastases, we used a transgenic mouse model where suppression of metastasis growth is lost due to gene knockout of the Pigment epithelium-derived factor (PEDF), also known as Serpin F1 (SERPINF1), a multifunctional secreted protein with anti-angiogenic and anti-tumorigenic functions [25]. In the *SerpinF1*$^{-/-}$ mouse model, metastasized melanoma cells immediately form large macro-metastases [26]. Remarkably, in this model, KCN1 completely inhibited growth of hepatic metastases (Fig. 2E), presumably by mimicking the biological function of PEDF in blocking micro- to macro-metastasis progression.

KCN1 inhibits eye tumor growth and extends survival in syngeneic and xenogeneic models of uveal melanoma

Next, we examined how KCN1 impacts survival in three orthotopic animal models: the B16LS9 model in immuno-competent C57BL/6 mice, and Mel290 and 92.1 human UM cell lines in immunocompromised (athymic nude) mice. Melanoma cells were inoculated in the uveal layer of the eye and the mice treated daily with i.p. KCN1 (60 mg/kg). Eyes were enucleated 7–9 days later and the average largest surface occupied by the tumor measured. Systemic treatment with KCN1 reduced the size of the intraocular tumor in all three models by ~60–75% (Fig. 3A). After enucleation, KCN1 treatment continued and the mice were followed for survival. Kaplan–Meier curves indicate that in all models KCN1 significantly extended mice survival (Fig. 3B).

In the 92.1 model substantial variation in survival time, heterogeneity in symptom development and additional phenotypic changes were observed. Livers of vehicle-treated animals displayed hepatic macro-metastases, necrosis, and hemorrhage, whereas in KCN1-treated animals only micro-metastases were detected (Supplementary Fig. 5A). Quantification indicated a significantly higher metastatic load in the liver of vehicle-treated animals (Supplementary Fig. 5B). In addition to liver, metastases were also detected in the lung and kidneys but not hearts of some animals, the percentage of incidence and the size being higher in control animals (Supplementary Fig. 6).

Altogether, these results show that KCN1 prevents formation of macro-metastases and functional damage to the liver and decreases hepatic micro-metastatic load, through therapeutic effects exerted both at the primary tumor and in metastatic events.

KCN1 is well-tolerated in the mouse uveal melanoma models

Up to at least 14 weeks of five injections of KCN1/week was well tolerated by the mice. No extraneous signs of toxicity were apparent; the animal bodily appearance, behavior, and activity were indistinguishable from untreated animals. No significant treatment-induced changes of body weight were observed throughout the experiment (Supplementary Fig. 7A). Pathological examination of main organs showed no treatment-related changes in the heart, kidney, spleen, lung, and gastrointestinal tract (Supplementary Fig. 7B). Liver swelling and

a more reddish color were observed at autopsy in all mice but was more pronounced in KCN1-treated animals. Pathology showed an accumulation of liquid within the bile ducts in all groups, yet without evidence for any hepatocytic death. Liver changes with KCN1 treatment are known [23, 27], and they are likely caused by the Cremophor EL/ethanol formulation [28].

KCN1 inhibits hypoxia-induced pro-invasive/metastatic signaling in melanoma cells and collagen maturation in UM tumors

To assess the role of P4HA1/2 in the hypoxia-induced motility of UM cells, and its inhibition by KCN1, we performed scratch wound migration assays over 48 h. KCN1 alone significantly reduced wound closure by about 50% (Fig. 4A, top). Single siRNA against P4HA1 or P4HA2 reduced migration by about 40%, while co-siRNA treatment reduced it by about 50%, suggesting that both enzymes play a role in hypoxia-induced migration. Combination of KCN1 and single P4HA1/2 knock-down did not offer additional inhibition, but KCN1 with dual knock-down of P4HA1 and P4HA2 was slightly more efficient, suggesting that KCN1 may have anti-migratory action beyond P4HA1/2 inhibition. Similar results were found in the Boyden chamber Matrigel invasion assay, but the inhibition was more profound with ~80% reduction (Fig. 4A bottom right and Supplementary Fig. 8). Inhibition of P4HA1 and 2 was confirmed by immunoblotting (Fig. 4A, bottom left). These findings establish that P4HA1/2 are critical for UM cell migration/invasion, a prerequisite for cancer cell metastasis, and KCN1 interferes with this process;in large part, through inhibiting P4HA1 and 2 expression.

We next examined the impact of KCN1 treatment on collagen maturation, a process that requires extensive hydroxylation of proline residues [16]. Examination of livers burdened by metastases showed a reduction in collagen deposition in KCN1-treated mice with 92.1 xenografts (Fig. 4B). Using a Sircol assay that can detect soluble collagens in CM, we found that cell secretion of collagen is induced by hypoxia and inhibited by KCN1 (Fig. 4C). Immunoblotting of the conditioned media (CM) from UM cells with an anti-hydroxyproline antibody detected a single band (~150kDa), the intensity of which was strongest under hypoxia and potently reduced by KCN1 (Fig. 4D, top).

Analysis of TCGA data showed that *col6A1* and *col6A2* are the most abundantly expressed collagen genes in UM (Supplementary Fig. 9). These respectively encode the α1 and α2 protein chains that form type VI collagen, a widely distributed ECM protein highly expressed in a variety of cancers that favors tumor growth and progression [29]. Western blot showed that the 150 kDa α1(VI) collagen chain could be detected in concentrated CM of UM cells in culture and its levels were decreased by KCN1 (Fig. 4D, top). Unexpectedly, KCN1 treatment also induced proteolytic cleavage of the α1 (VI) chain, both in vitro (Fig. 4D, top) and in primary eye tumor lysate (Fig. 4D, bottom left). Moreover, analysis under native conditions showed that KCN1 induced aberrant aggregation of collagen type VI as evidenced by a large range of sizes of assembled collagen complexes (Fig. 4D, bottom right). These results may reflect type VI collagen instability and misfolding induced by improper hydroxylation and cleaved α chains.

Altogether, these data indicate that KCN1 potently downregulates hypoxia-activated invasion/metastasis-promoting genes P4HA1 and 2, and disrupts collagen secretion/deposition in UM by interfering with its proper posttranslational modification and inducing its proteolysis.

DISCUSSION

In this report, we demonstrate the therapeutic potential of targeting hypoxia-induced pro-invasive/metastatic genes in UM. In particular, our analyses identified collagen synthesis genes P4HA1 and 2 to be potently activated by hypoxia in UM cells and their expression was strongly correlated with patient metastatic progression and survival. These findings suggest that P4HA1/2 could serve as prognostic markers. We demonstrated that hypoxia-mediated activation of P4HA1 and P4HA2 enzymes could be reduced by a small molecule HIF inhibitor (KCN1), resulting in potent antitumor activity and increased animal survival in three different orthotopic mice models of UM. The treatment reduced disease burden both at the primary tumor site and against distant metastases in the liver and other organs. These results are important because the development of novel systemic chemotherapy to treat UMs while preserving vision and preventing death from metastasis is urgently needed [30].

KCN1 was most effective at reducing metastasis upon early administration, suggesting that by reducing eye tumor burden and tumor cell invasive behavior, it lessens escape of melanoma cells from the primary tumor. This demonstrates the importance of early detection and rapidly controlling primary tumor size. Yet, even when treatment was not started until the primary tumors were removed, KCN1 still inhibited metastases independently. This data suggests that KCN1 also impacts metastasis directly in the liver, by blocking the progression of seeded melanoma cells into micro- and macro-metastases. Remarkably, in the *SerpinF1* knockout UM mouse model [26], where the suppressive effects of hepatocyte-secreted PEDF against micro- to macro-metastasis progression are removed, KCN1 fully substituted for them and kept the disease microscopic, demonstrating its antimetastatic potency and the potential of this chemotype as a metastasis growth prevention agent. KCN1 is a small (MW: 465.572), chemically stable arylsulfonamide, sufficiently lipophilic to ensure good cell membrane penetration and our microPET in vivo distribution analysis demonstrates that it distributes well to both the eyes and liver. While KCN1 is well-tolerated in mice and has desirable pharmaceutical properties [24], further optimization of this class of compounds is needed before they can reach the clinic. Improved solubility is necessary and we are performing additional chemistry to enhance hydrophilicity [20, 21, 31, 32] and are testing new formulations that avoid the use of alcohol to reduce liver burden [27, 33].

Hypoxia-induced collagen production, and related ECM remodeling are needed for cancer invasion and metastasis [15, 17, 18]. P4HA1 and 2 are key enzymes involved in collagen hydroxylation, which is an essential step in enabling its maturation and secretion [16]. Both enzymes are upregulated by hypoxia [34–37]. At the molecular level, KCN1 inhibition of hypoxia-activated *P4HA1/2* transcription, resulted in decreased levels of secreted proline-hydroxylated collagen as anticipated, but unexpectedly also induced proteolytic cleavage of α1(VI) and resulted in completely disordered collagen VI assembly, the major form of collagen produced by UM tumors. Further studies are needed to identify the mechanism

underlying this cleavage and how it relates to hypo-prolyl hydroxylation of α1(VI). Whether the deposition of the extracellular collagen matrix disrupted by KCN1 is most relevant for tumor cell escape from the primary eye tumor, or for the establishment and progression of micro-metastases through ECM remodeling of the metastatic tissue also remains to be established.

In summary, we demonstrate that P4HA1/2 gene expression correlates with patient metastasis and survival, supporting their use as prognostic markers. Transcriptional targeting of hypoxia-mediated upregulation of these enzymes with a HIF inhibitor is feasible and results in major disruption of collagen fiber synthesis and orderly matrix deposition. The treatment had potent anti-eye tumor, anti-invasion/metastasis, and anti-ECM activities in pre-clinical orthotopic UM models, supporting P4HA1/2 therapeutic targeting. Now that patients at high risk for metastasis can be identified using a series of markers in the primary eye tumor [38], it is conceivable to put patients on a neoadjuvant metastasis prevention therapy. Our study suggests that KCN1 has desirable properties as a suppressor of metastasis: it is well tolerated, has excellent distribution to the eye and the liver, and is thus ideally suited for treating metastatic UM. Overall, our preclinical studies support the further translation of the arylsulfonamide scaffold toward a novel treatment for patients with metastatic UM.

MATERIALS AND METHODS

KCN1 synthesis, formulation, microPET, and pharmacokinetic analysis

Synthesis and purification of >99% pure 3,4-dimethoxy-N-[(2,2-dimethyl-2H-chromen-6-yl)methyl]-N-phenylbenzenesulfonamide (KCN1) was described [23]. Preparation of KCN1 for animal experiments is described in Supplementary Methods. Radiochemical synthesis of [^{11}C]KCN1 and micro-positron emission tomography (microPET) procedure are described in Supplementary Methods. Pharmacokinetic analysis was described previously [24].

Cell culture

Human UM cell lines Mel290, 92.1, OCM1, OMM1, and OMM2-5, and the mouse melanoma cell line B16LS9 were obtained from sources described in Acknowledgments. All cell lines were cultured under conditions previously described [39]. Human cells were authenticated by genetic testing (Emory Integrated Genomics Core, Supplementary Table 1) and all cells tested free of mycoplasma. Cells were pre-treated with indicated concentrations of KCN1 or vehicle (1% DMSO final concentration in media) for 1 h under normoxia (21% O_2) and then incubation continued under normoxia or hypoxia (1% O_2) using a hypoxia incubator (Thermo Forma, Model 3130, Thermo Fisher Scientific, Waltham, MA, USA).

Transfection of short interfering RNA (siRNA)

Cells were plated 24 h prior transfection and treated with control, *P4HA1, P4HA2* (SR30004, SR303331A, and SR322607A, OriGene Technologies, Rockville, MD, USA), *HIF1A* (sc-45919, Santa Cruz Biotechnology, Dallas, TX, USA), and *EPAS1* (AM16708, Thermo Fisher Scientific)-targeting siRNAs using Lipofectamine RNAiMAX Reagent (Thermo Fisher Scientific) as recommended.

Preparation of cell lysates and western blot

Cells were washed with cold PBS and immediately lysed in 1X SDS-PAGE Loading Buffer (63mM Tris-HCl, pH 6.8, 2% (w/v) SDS, 10% glycerol, 0.01% (w/v) bromophenol blue, and 40mM dithiothreitol). Total cell lysates were separated by SDS-PAGE, transferred to a nitrocellulose membrane and probed with HIF-1α (human: 610958, BD Biosciences, San Jose, CA, USA; mouse: ab2185, Abcam, Cambridge, UK), HIF-2α (AF2997, R&D Systems, Minneapolis, MN, USA), P4HA1 (NBP1-84398, Novus Biologicals, Centennial, CO, USA), P4HA2 (MA5-24599, Thermo Fisher Scientific), anti-hydroxyproline (ab37067, Abcam), Col6A1 (A9236, ABclonal, Woburn, MA, USA), Galectin 3 (PA5-80773, Thermo Fisher Scientific), and β-actin (#4970, Cell Signaling Technology, Danvers, MA, USA) antibodies. Detection was as described previously [23]. Signal intensity was quantitated by ImageJ (Rasband, W.S., ImageJ, U. S. National Institutes of Health, Bethesda, Maryland, USA, https://imagej.nih.gov/ij/, 1997–2018).

Preparation of conditioned medium (CM)

UM cells (5×10^6 in 10 cm diameter dish, 15 ml serum-free medium) were incubated in normoxia/hypoxia ± 10 μM KCN1 for 60 h, medium was recovered, cleared by centrifugation, and precipitated overnight in ice with $(NH_4)_2SO_4$ (80% final concentration). Precipitate was recovered by centrifugation (12,000 *rpm,* 20 min), briefly dried, dissolved in 120 μl of PBS, and 30 ug of protein/sample were analyzed by PAGE under denaturing/reducing conditions (samples heated at 95 °C for 5 min in 62.5 mM Tris-HCl, 2% SDS, 10% glycerol, 50 mM DTT, 0.01% bromophenol blue and separated in Tris/glycine/SDS buffer) or native conditions (samples loaded without heating in 30mM Tris-HCl, pH 6.8, 20% glycerol, 0.01% bromophenol blue, and run in Tris/glycine buffer).

In vitro scratch wound cell migration assay

92.1 cells in 24-well plates were transfected with control, P4HA1, or P4HA2-targeting siRNAs using Lipofectamine RNAiMAX Reagent as recommended. After 24 h, a p200 pipet tip was used to create a scratch in the cell monolayer, cells were washed once with PBS, incubated for 48 h in regular medium, then washed once with PBS, images taken and width of wound analyzed by ImageJ.

Modified Boyden chamber assay

92.1 cells in 24-well plates were seeded a day before transfection. Cells were transfected with control, *P4HA1,* or *P4HA2*-targeting siRNAs using Lipofectamine RNAiMAX Reagent as recommended. After 24 h, the cells were harvested using cell dissociation buffer (13151-014, Life Technologies) and 0.3×10^5 cells were transferred to the upper chamber (Cell culture insert, 24-well format, 8.0 μm pore size, 353097, Corning, Corning, NY, USA) with 150 μL of serum free RPMI1640 medium. 500 μL of RPMI1640 containing 10% FBS and ±10 μM KCN1 were added to the lower chamber of the 24-well plate and pre-incubated for 1 h under normoxia. The plate was then transferred to a hypoxia incubator (1% O_2) for 48 h. The cells on the upper side of the membrane were removed with a cotton swab, after which the membrane was fixed and stained with a 0.05% Crystal violet (V5265, Sigma-Aldrich, St. Louis, MO, USA); 1% methanol (A452, Thermo Fisher Scientific); 1%

Formaldehyde (BP531, Thermo Fisher Scientific) solution for 30 min. Subsequently, images of the cells migrated to the lower side of the membrane were taken and analyzed by ImageJ.

Collagen assay

Collagen in CM was measured with Sircol™ Soluble Collagen Assay (Biocolor, Carrickfergus, UK) as recommended.

RNA extraction and qRT-PCR

Total RNA was extracted using TRIzol™ Reagent (Thermo Fisher Scientific) and 1st strand cDNA was synthesized with the ProtoScript First Strand cDNA Synthesis Kit (New England Biolabs, Ipswich, MA, USA). Amplifications were performed in 7500 Fast Real-Time PCR System (Applied Biosystems, Thermo Fisher Scientific) using SYBR Green chemistry (Applied Biosystems) and human or mouse gene-specific primers (Supplementary Table 2A, B). *β-actin* was used as internal control and data were analyzed with 7500 Software, v2.3. Heatmaps were generated using Morpheus software (https://software.broadinstitute.org/morpheus).

Microarray analysis

GSE27831 [40] and GSE22138 [41] microarray datasets (Affymetrix U133_plus2 platform) were downloaded from the Gene Expression Omnibus database (http://www.ncbi.nlm.nih.gov/geo/). Merged expression and raw expression data (CEL files) were summarized and normalized using the Robust Multi-array Average algorithm (http://www.bioconductor.org/packages/2.0/bioc/html/affy.html) from the Bioconductor library for the R statistical programming system. TIBCO Spotfire software package (TIBCO Software, Palo Alto, CA, USA) was used for heatmap visualization of mRNA expression.

Outcome analysis

Survival data analysis of UM patients from the TCGA database [10] was performed by using PROGgeneV2 (http://genomics.jefferson.edu/proggene/index.php) platform database [42]. High/Low are defined as median value.

Identification of hypoxia responsive elements (HRE)

The Integrative Genomic Viewer software [43] was used to visualize the location of *P4HA1* and *P4HA2* HREs. HREs were mapped to the human reference genome GRCh37/hg19.

Uveal melanoma mouse models

Twelve-week-old female C57BL/6 (Charles River Laboratories, Wilmington, MA, USA) or nu/nu (The Jackson Laboratory, Bar Harbor, ME, USA) mice (10–15 mice/group) were used under IACUC approval and adherence to the NIH Guide for the Care and Use of Laboratory Animals. Individual mice were marked with ear tags (C57BL/6) or skin tattoos (nude) [44]. On day 0, melanoma cells were inoculated into the supra-choroidal space of the right murine eye using a trans-scleral technique as previously described [39]. Mice were randomly assigned to control and drug treatment groups. KCN1 in a 1:1 Cremophor EL/ethanol formulation (Supplementary Methods) was administered by intraperitoneal (i.p.)

injection at 30 or 60 mg/kg daily or twice/day for 5 days/week. For the B16LS9 model, treatments started on days 1, 4, or 7 after tumor inoculation. Tumor-bearing eyes were enucleated on the 7th day after inoculation, and the livers were collected at the time of sacrifice on the 28th day after inoculation. For the Kaplan–Meier survival experiments with B16LS9 and Mel290, the mice underwent enucleation on day 7 and then were observed until reaching IACUC criteria for termination. KCN1 was administered during the whole time. In the 92.1 experiment, mice were enucleated on day 9, KCN1 was administered for 14 weeks, and then observed until reaching IACUC criteria for termination. Animal weight was monitored weekly. Harvested eyes, livers, and other tissues were prepared for pathological examinations as previously described [39].

Masson's trichrome staining

Masson's staining was performed with Trichrome, Masson, Aniline Blue Stain Kit (Newcomer Supply, Middleton, WI, USA). Stained slides were scanned using NanoZoomer 2.0-HT (Hamamatsu Photonics, Hamamatsu, Japan) and analyzed by Aperio ImageScope [v12.3.2.8013] (Leica Biosystems Imaging, Buffalo Grove, IL, USA).

Statistical analyses

Differences between two groups were analyzed using two-sided unpaired Student's *t* test. Differences between three or more groups were analyzed using one-way ANOVA. *P* values < 0.05 were considered statistically significant. Statistical analyses were performed with Graphpad Prism 5 software (San Diego, CA, USA).

For the animal survival studies, we used the Kaplan–Meier method and the log-rank test to test for a significant difference in survival distributions between the drug-treated and control groups. With ten mice/group, we have 80% power to detect a hazard ratio of 4.24 assuming a Type I error of 0.05 using a log-rank test. With ten mice/group, we have 80% power to detect an effect size of 1.3 when comparing tumor size between groups using a two-sample *t*-test based on our prior studies [33].

Supplementary Material

Refer to Web version on PubMed Central for supplementary material.

ACKNOWLEDGEMENTS

We thank Dr Bruce Ksander (Schepens Eye Institute, Boston, MA) for providing Mel290 and OMM2-5 cells (OMM2-5 was established by Dr Timothy Murray, Bascom Palmer Eye Institute, Miami, FL); Dr Jerry Niederkorn (Department of Ophthalmology, UT Southwestern, Dallas, TX) for OMM1 and 92.1 cells (92.1 cells were established by Dr Gregorius P. Luyten, Department of Ophthalmology, Rotterdam University Hospital); Dr June Kan-Mitchel (Wayne State University, Detroit, MI) for OCM1 cells, and Dr Dario Rusciano (Friedrich Miescher Institute, Basel, Switzerland) for providing B16LS9 cells. We thank the Winship Research Pathology Core Lab (Emory University) for IHC and Masson's staining. We also acknowledge Zhengjia Chen (Department of Biostatistics & Bioinformatics, Emory Rollins School of Public Health) for providing statistical consultation. We appreciate the helpful advice and assistance of all members of the Laboratory of Molecular Neuro-Oncology.

FUNDING

This work was supported in part by grants from the NIH (R01 CA116804, R01 CA176001, R01 CA180805, R24 EY017045, P30 EY06360, P30 CA138292 and P30 CA13148), the National Natural Science Foundation of

China (NNS81201808), the Fight For Sight Postdoctoral Award, the Emory Melanoma Prevention and Research Discovery Fund, a Winship Cancer Institute pilot grant, a Central South University Lieying pilot grant, the V Foundation, the Max Cure Foundation, the Samuel Waxman Cancer Research Foundation, the Alan B. Slifka Foundation, and an unrestricted grant from Research to Prevent Blindness, Inc.

REFERENCES

1. Siegel R, Naishadham D, Jemal A. Cancer statistics, 2012. CA Cancer J Clin. 2012;62:10–29. [PubMed: 22237781]
2. Harbour JW, Chao DL. A molecular revolution in uveal melanoma: implications for patient care and targeted therapy. Ophthalmology. 2014;121:1281–8. [PubMed: 24480708]
3. Chattopadhyay C, Kim DW, Gombos DS, Oba J, Qin Y, Williams MD, et al. Uveal melanoma: from diagnosis to treatment and the science in between. Cancer. 2016;122:2299–312. [PubMed: 26991400]
4. Dogrusoz M, Jager MJ. Genetic prognostication in uveal melanoma. Acta Ophthalmol. 2018;96:331–47. [PubMed: 29105334]
5. Sullivan RJ, Flaherty KT. New strategies in melanoma: entering the era of combinatorial therapy. Clinical cancer research: an official journal of the American Association for. Cancer Res. 2015;21:2424–35.
6. Klein CA. Cancer. The metastasis cascade. Science. 2008;321:1785–7. [PubMed: 18818347]
7. Chiang AC, Massague J. Molecular basis of metastasis. N Engl J Med. 2008;359:2814–23. [PubMed: 19109576]
8. Joyce JA, Pollard JW. Microenvironmental regulation of metastasis. Nat Rev Cancer. 2009;9:239–52. [PubMed: 19279573]
9. Rankin EB, Giaccia AJ. Hypoxic control of metastasis. Science. 2016;352:175–80. [PubMed: 27124451]
10. Robertson AG, Shih J,Yau C, Gibb EA, Oba J, Mungall KL, et al. Integrative Analysis Identifies Four Molecular and Clinical Subsets in Uveal Melanoma. Cancer Cell. 2017;32:204–20. e215 [PubMed: 28810145]
11. Mouriaux F, Sanschagrin F, Diorio C, Landreville S, Comoz F, Petit E, et al. Increased HIF-1alpha expression correlates with cell proliferation and vascular markers CD31 and VEGF-A in uveal melanoma. Investig Ophthalmol Vis Sci. 2014;55:1277–83. [PubMed: 24481264]
12. Asnaghi L, Lin MH, Lim KS, Lim KJ, Tripathy A, Wendeborn M, et al. Hypoxia promotes uveal melanoma invasion through enhanced Notch and MAPK activation. PLoS ONE. 2014;9:e105372. [PubMed: 25166211]
13. Hu K, Babapoor-Farrokhran S, Rodrigues M, Deshpande M, Puchner B, Kashiwabuchi F, et al. Hypoxia-inducible factor 1 upregulation of both VEGF and ANGPTL4 is required to promote the angiogenic phenotype in uveal melanoma. Oncotarget. 2016;7:7816–28. [PubMed: 26761211]
14. el Filali M, Missotten GS, Maat W, Ly LV, Luyten GP, van der Velden PA, et al. Regulation of VEGF-A in uveal melanoma. Investig Ophthalmol Vis Sci. 2010;51:2329–37. [PubMed: 20042655]
15. Provenzano PP, Eliceiri KW, Campbell JM, Inman DR, White JG, Keely PJ. Collagen reorganization at the tumor-stromal interface facilitates local invasion. BMC Med. 2006;4:38. [PubMed: 17190588]
16. Canty EG, Kadler KE. Procollagen trafficking, processing and fibrillogenesis. J Cell Sci. 2005;118:1341–53. [PubMed: 15788652]
17. Gilkes DM, Chaturvedi P, Bajpai S, Wong CC, Wei H, Pitcairn S, et al. Collagen prolyl hydroxylases are essential for breast cancer metastasis. Cancer Res. 2013;73:3285–96. [PubMed: 23539444]
18. Xiong G, Deng L, Zhu J, Rychahou PG, Xu R. Prolyl-4-hydroxylase alpha subunit 2 promotes breast cancer progression and metastasis by regulating collagen deposition. BMC Cancer. 2014;14:1. [PubMed: 24383403]
19. Walker C, Mojares E, Del Rio Hernandez A. Role of Extracellular Matrix in Development and Cancer Progression. Int J Mol Sci. 2018 Oct 4;19:3028.

20. Mun J, Jabbar AA, Devi NS, Liu Y, Van Meir EG, Goodman MM. Structure–activity relationship of 2,2-dimethyl-2H-chromene based arylsulfonamide analogs of 3,4-dimethoxy-N-[(2,2-dimethyl-2H-chromen-6-yl)methyl]-N-phenylbenzenesulfonamide, a novel small molecule hypoxia inducible factor-1 (HIF-1) pathway inhibitor and anti-cancer agent. Bioorg Med Chem. 2012;20:4590–7. [PubMed: 22682301]
21. Mooring SR, Jin H, Devi NS, Jabbar AA, Kaluz S, Liu Y, et al. Design and Synthesis of Novel Small-Molecule Inhibitors of the Hypoxia Inducible Factor Pathway. J Med Chem. 2011;54:8471–89. [PubMed: 22032632]
22. Shi Q, Yin S, Kaluz S, Ni N, Devi NS, Mun J, et al. Binding Model for the Interaction of Anticancer Arylsulfonamides with the p300 Transcription Cofactor. ACS Med Chem Lett. 2012;3:620–5. [PubMed: 24936238]
23. Yin S, Kaluz S, Devi NS, Jabbar AA, de Noronha RG, Mun J, et al. Arylsulfonamide KCN1 Inhibits In Vivo Glioma Growth and Interferes with HIF Signaling by Disrupting HIF-1 alpha Interaction with Cofactors p300/CBP. Clin Cancer Res. 2012;18:6623–33. [PubMed: 22923450]
24. Wang W, Ao L, Rayburn ER, Xu H, Zhang X, Zhang X et al. KCN1, a Novel Synthetic Sulfonamide Anticancer Agent: in Vitro and In Vivo Anti-Pancreatic Cancer Activities and Preclinical Pharmacology. PLoS ONE.2012;7:e44883. [PubMed: 23028659]
25. Filleur S, Nelius T, de Riese W, Kennedy RC. Characterization of PEDF: a multi-functional serpin family protein. J Cell Biochem. 2009;106:769–75. [PubMed: 19180572]
26. Lattier JM, Yang H, Crawford S, Grossniklaus HE. Host pigment epithelium-derived factor (PEDF) prevents progression of liver metastasis in a mouse model of uveal melanoma. Clin Exp Metastasis. 2013;30:969–76. [PubMed: 23793989]
27. Dai X, Kaluz S, Jiang Y, Shi L, McKinley D, Wang Y, et al. A novel small-molecule arylsulfonamide causes energetic stress and suppresses breast and lung tumor growth and metastasis. Oncotarget. 2017;8:99245–60. [PubMed: 29245898]
28. Gelderblom H, Verweij J, Nooter K, Sparreboom A, Cremophor EL. The drawbacks and advantages of vehicle selection for drug formulation. Eur J Cancer. 2001;37:1590–8. [PubMed: 11527683]
29. Chen P, Cescon M, Bonaldo P. Collagen VI in cancer and its biological mechanisms. Trends Mol Med. 2013;19:410–7. [PubMed: 23639582]
30. Diener-West M, Earle JD, Fine SL, Hawkins BS, Moy CS, Reynolds SM, et al. The COMS randomized trial of iodine 125 brachytherapy for choroidal melanoma, III: initial mortality findings. COMS Report No. 18. Arch Ophthalmol. 2001;119:969–82. [PubMed: 11448319]
31. Ferguson JH, De Los Santos Z, Devi SN, Kaluz S, Van Meir EG, Zingales SK, et al. Design and synthesis of benzopyran-based inhibitors of the hypoxia-inducible factor-1 pathway with improved water solubility. J Enzym Inhib Med Chem. 2017;32:992–1001.
32. Tan C, de Noronha RG, Devi NS, Jabbar AA, Kaluz S, Liu Y, et al. Sulfonamides as a new scaffold for hypoxia inducible factor pathway inhibitors. Bioorg Med Chem Lett. 2011;21:5528–32. [PubMed: 21831638]
33. Dong L, You S, Zhang Q, Osuka S, Devi NS, Kaluz S, et al. Arylsulfonamide 64B Inhibits Hypoxia/HIF-Induced Expression of c-Met and CXCR4 and Reduces Primary Tumor Growth and Metastasis of Uveal Melanoma. Clin Cancer Res. 2019;25:2206–18. [PubMed: 30563937]
34. Hofbauer KH, Gess B, Lohaus C, Meyer HE, Katschinski D, Kurtz A. Oxygen tension regulates the expression of a group of procollagen hydroxylases. Eur J Biochem. 2003;270:4515–22. [PubMed: 14622280]
35. Grimmer C, Balbus N, Lang U, Aigner T, Cramer T, Muller L, et al. Regulation of type II collagen synthesis during osteoarthritis by prolyl-4-hydroxylases: possible influence of low oxygen levels. Am J Pathol. 2006;169:491–502. [PubMed: 16877351]
36. Stegen S, Laperre K, Eelen G, Rinaldi G, Fraisl P, Torrekens S, et al. HIF-1alpha metabolically controls collagen synthesis and modification in chondrocytes. Nature. 2019;565:511–5. [PubMed: 30651640]
37. Gilkes DM, Bajpai S, Chaturvedi P, Wirtz D, Semenza GL. Hypoxia-inducible factor 1 (HIF-1) promotes extracellular matrix remodeling under hypoxic conditions by inducing P4HA1, P4HA2, and PLOD2 expression in fibroblasts. J Biol Chem. 2013;288:10819–29. [PubMed: 23423382]

38. Onken MD, Worley LA, Davila RM, Char DH, Harbour JW. Prognostic testing in uveal melanoma by transcriptomic profiling of fine needle biopsy specimens. J Mol Diagn. 2006;8:567–73. [PubMed: 17065425]

39. Zhang Q, Yang H, Kang SJ, Wang Y, Wang GD, Coulthard T, et al. In vivo high-frequency, contrast-enhanced ultrasonography of uveal melanoma in mice: imaging features and histopathologic correlations. Investig Ophthalmol Vis Sci. 2011;52:2662–8. [PubMed: 21245408]

40. Gangemi R, Mirisola V, Barisione G, Fabbi M, Brizzolara A, Lanza F, et al. Mda-9/syntenin is expressed in uveal melanoma and correlates with metastatic progression. PloS ONE. 2012;7:e29989. [PubMed: 22267972]

41. Laurent C, Valet F, Planque N, Silveri L, Maacha S, Anezo O, et al. High PTP4A3 phosphatase expression correlates with metastatic risk in uveal melanoma patients. Cancer Res. 2011;71:666–74. [PubMed: 21135111]

42. Goswami CP, Nakshatri H. PROGgeneV2: enhancements on the existing database. BMC Cancer. 2014;14:970. [PubMed: 25518851]

43. Robinson JT, Thorvaldsdottir H, Winckler W, Guttman M, Lander ES, Getz G, et al. Integrative genomics viewer. Nat Biotechnol. 2011;29:24–26. [PubMed: 21221095]

44. Van Meir EG. Identification of nude mice in tumorigenicity assays. Int J Cancer. 1997;71:310. [PubMed: 9139859]

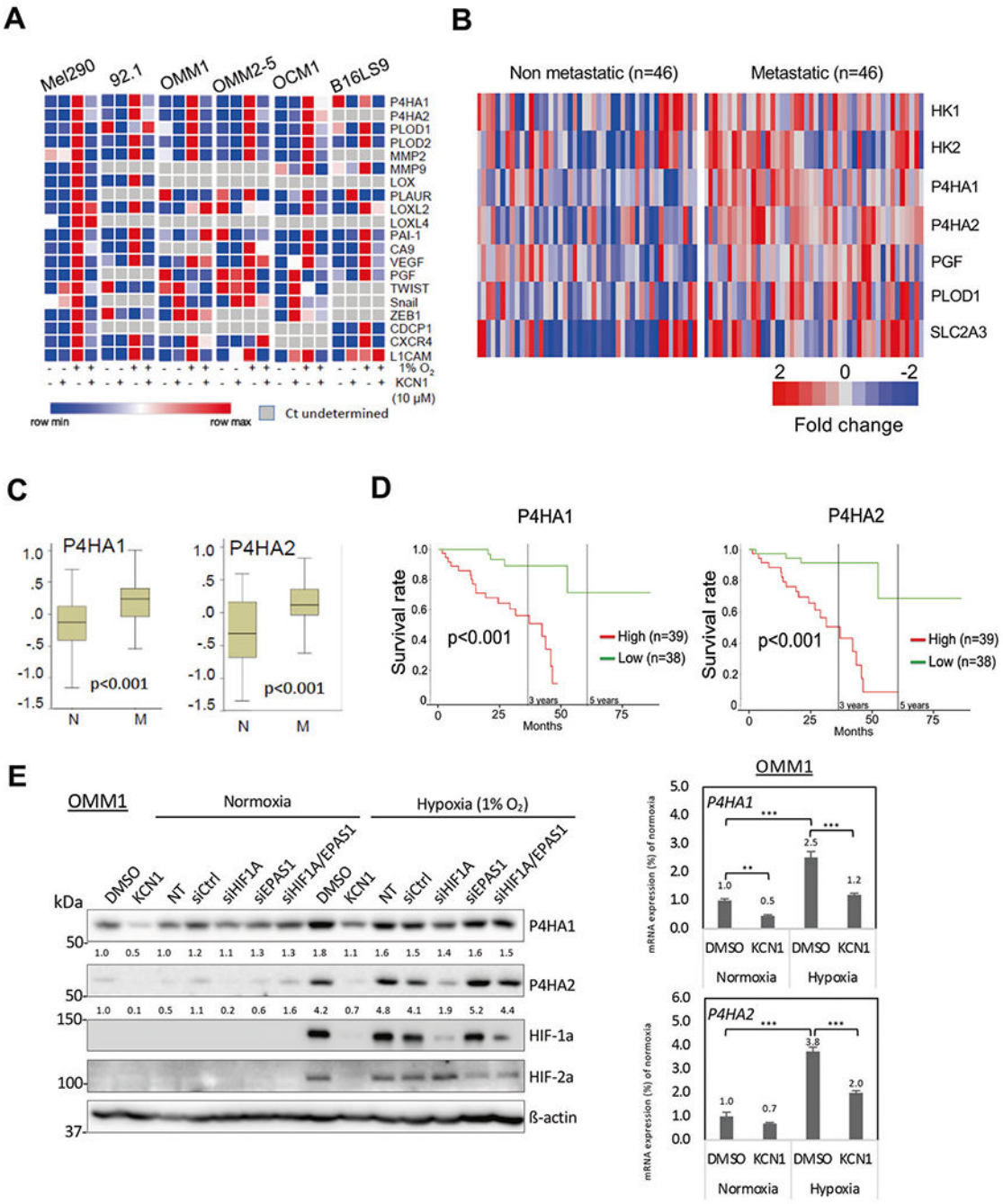

Fig. 1. Expression of hypoxia-inducible metastasis-related genes in UM patient eye tumors and cell lines.

A Heatmap of qRT-PCR data probing expression of hypoxia-inducible pro-metastatic genes in melanoma cell lines ± KCN1 treatment (10μM). *β-actin* was used as internal control and results are expressed as fold change over normoxic control. Data are presented as relative expression (min/max in each row). **B** Heatmap showing hypoxia-inducible metastasis-related genes that display significantly altered expression between UM patients with non-metastatic versus metastatic disease. Microarray datasets (GSE27831 and GSE22138) were used (see

Methods). **C** Relative expression of *P4HA1/2* genes in non-metastatic (N) and metastatic (M) uveal melanoma patients. Data were generated by analyzing combined datasets GSE27831 and GSE22138. Mann–Whitney U-test was used to compare both groups and determine *p* values. **D** Overall survival of UM patients with high and low expression of *P4HA1/2* genes. Kaplan–Meier survival curves were generated by analyzing UM cases deposited in the TCGA database. Log-rank test was used to compare survival between the two groups. **E** Hypoxia-induced expression of P4HA1 and P4HA2 mRNA and protein in OMM1 cells. Left panel: For drug treatment, cells were cultured in normoxia or hypoxia (1% O_2) and treated with vehicle (0.1% DMSO) or KCN1 (10 μM) for 24 h. For RNAi-mediated silencing, cells were transfected with siCtrl, si*HIF1A*, si*EPAS1*, or si*HIF1A*/si*EPAS1* for 24 h, and subsequently cultured under normoxia or hypoxia (1% O_2) for 24 h. Proteins were detected by Western blot (8% gel), and signal intensity was quantified by Image J, normalized to β-actin levels, and numbers indicate fold change over normoxic control. Right panel: Relative mRNA expression of *P4HA1/2* genes in vehicle (0.1% DMSO) or KCN1 (10 μM) treated-OMM1 cells (48 h). *β-actin* was used as loading control and the numbers indicate fold change over normoxic control (** $p < 0.01$, *** $p < 0.001$ by Tukey's test). Representative result shown of three independent biological replicates.

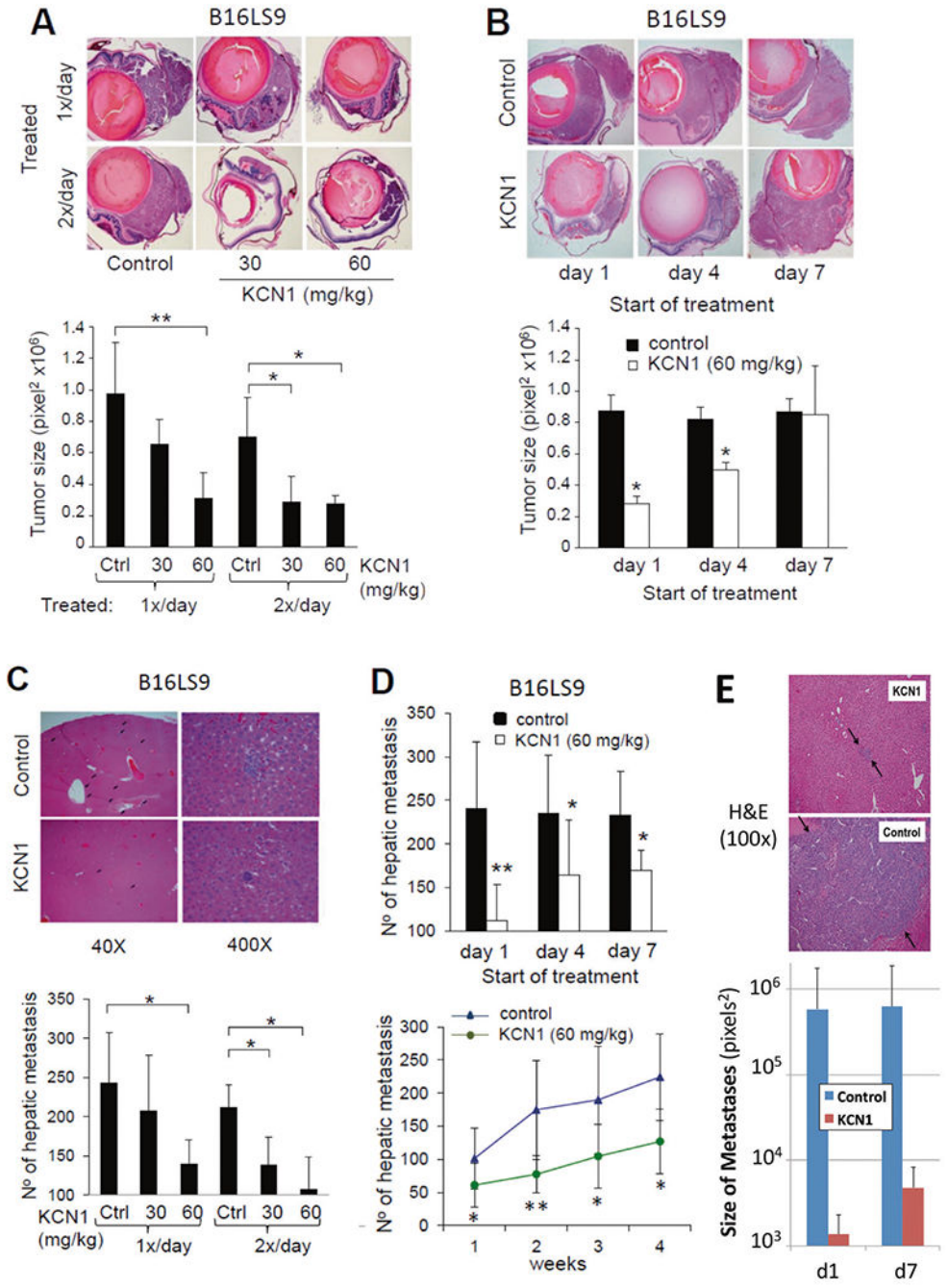

Fig. 2. KCN1 inhibits primary ocular tumor growth and formation of hepatic metastases in vivo.

B16LS9 melanoma cells were inoculated into the right eyes of C57Bl/6 mice, treatment with KCN1 (i.p., in a 1:1 Cremophor EL/ethanol formulation, controls vehicle only) started at day 1 post-inoculation, and tumor-burdened eyes were enucleated on day 7. Primary tumor burden was estimated by measuring the largest surface area of tumor. On day 28, mice were sacrificed and the livers were collected for enumeration of hepatic metastases. **A** Representative images of eye sections with melanoma ± KCN1 treatment (30 or 60 mg/kg i.p. daily, or twice daily from day 1; 5 days/week) (top, H&E staining, 40×).

Sections with the largest tumor area in each eye were used for quantifying tumor burden based on surface area (bottom, $n = 10$ mice/group. *$p < 0.05$, **$p < 0.01$ by ANOVA test). **B** Representative images (top, H&E staining, 40×) and quantification of reduction in eye tumor size with KCN1 treatment (60 mg/kg daily; 5 days/week) starting on days 1, 4 or 7 post-inoculation (bottom, $n = 10$ mice/group. *$p < 0.05$ by ANOVA test). **C** Liver histology at day 28 shows a reduction in hepatic micro-metastases in KCN1 (60 mg/kg daily from day 1; 5 days/week)-treated mice (top, H&E staining). Quantification of the number of hepatic metastases in mice from panel A. after 28 days of treatment (bottom, $n = 10$ mice/group. *$p < 0.05$ by ANOVA test). **D** Systemic KCN1 delivery in mice from panel B reduces the number of hepatic metastases by up to 60% at 28 days, and is most efficacious when treatment is started on day 1 post-tumor cell inoculation (top, $n = 10$ mice/group. *$p < 0.05$, **$p < 0.01$ by ANOVA test). Examination of liver metastatic colony load at 1–4 weeks post-inoculation shows antimetastatic effect of KCN1 (60 mg/kg twice daily; 5 days/week) holds longitudinally (bottom, $n = 10$ mice/group. *$p < 0.05$, **$p < 0.01$ by ANOVA test). **E** KCN1 inhibits micro- to macro-metastases progression of melanoma cells in livers of *SerpinF1*$^{-/-}$ mice. KCN1-treated *SerpinF1*$^{-/-}$ mice exhibited small, avascular micrometastases in the liver, while vehicle (Cremophor-EL/ethanol; 1:1) treated mice exhibited large vascularized >200 μm metastases (top panel). KCN1 treatment starting on the 1st or 7th day post-inoculation strongly reduced the size of the liver metastases by 100–1000 fold (bottom panel, $p = 0.04$ and $p = 0.03$ by ANOVA test, size in pixels^2 on log scale).

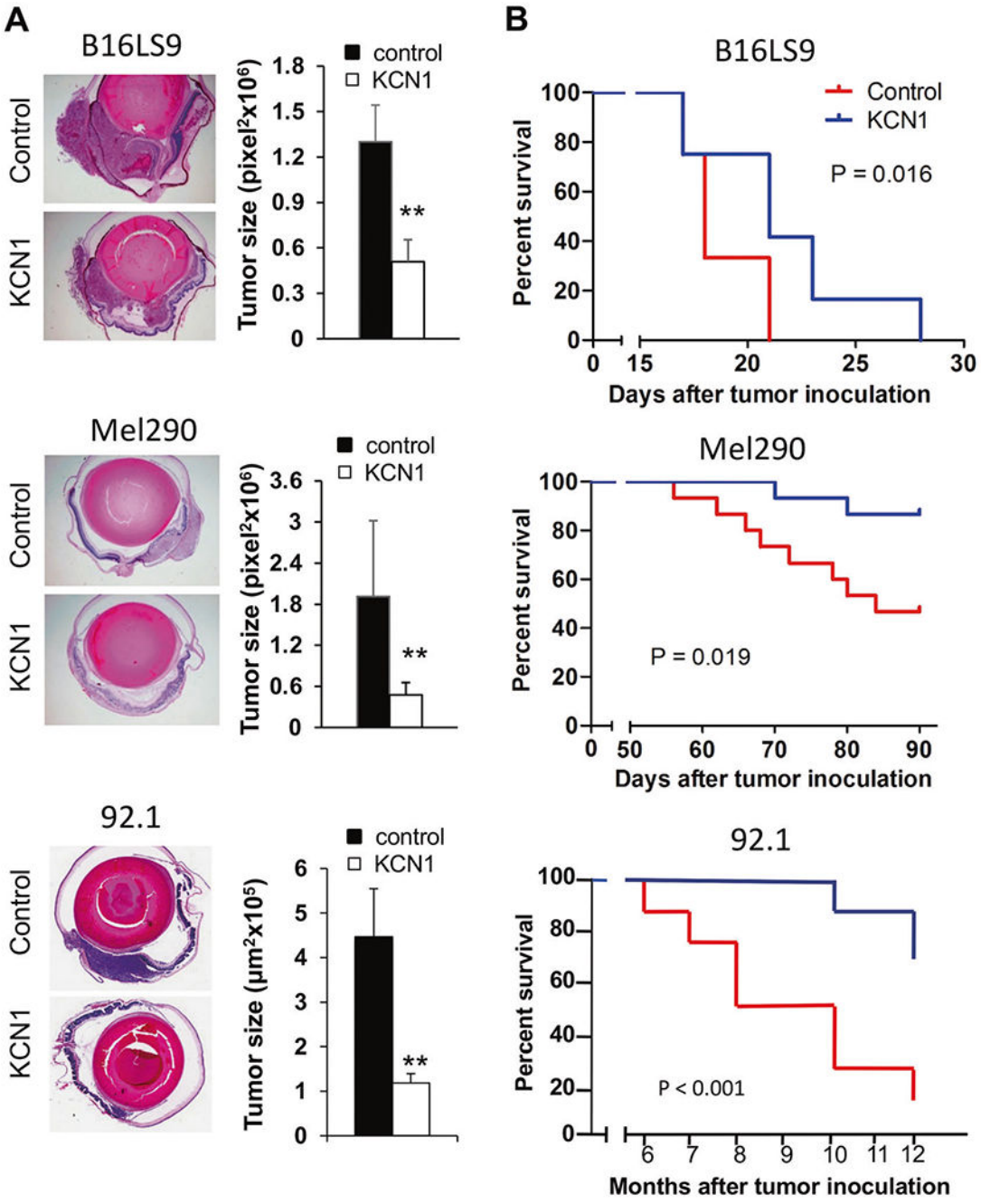

Fig. 3. KCN1 extends survival in orthotopic mouse models of uveal melanoma.

A B16LS9 mouse melanoma, Mel290 and 92.1 human UM cells were inoculated into the right eyes of C57BL/6 or nude mice, respectively. Treatment with KCN1 (i.p., 60 mg/kg daily; 5 days/week) was started at day 1 post-inoculation. Tumor-burdened eyes were enucleated on day 7 (B16LS9, Mel290) or day 9 (92.1). Representative images of B16LS9 (top), Mel290 (middle), and 92.1 (bottom) melanomas growing in the eye (left, H&E staining, 40×) and estimates of tumor burden by measuring the largest surface area of tumor show reduced primary eye tumor growth (right, $n = 10$ mice/group. $^{**}p < 0.01$

by two-tailed Student's *t* test). **B** Kaplan–Meier curves on enucleated mice from A. show that KCN1 extends the survival of mice burdened with metastatic melanoma . Mice were euthanized once they reached IACUC endpoint criteria (n = 10–15 mice/group, $p < 0.05$ by Log-rank test).

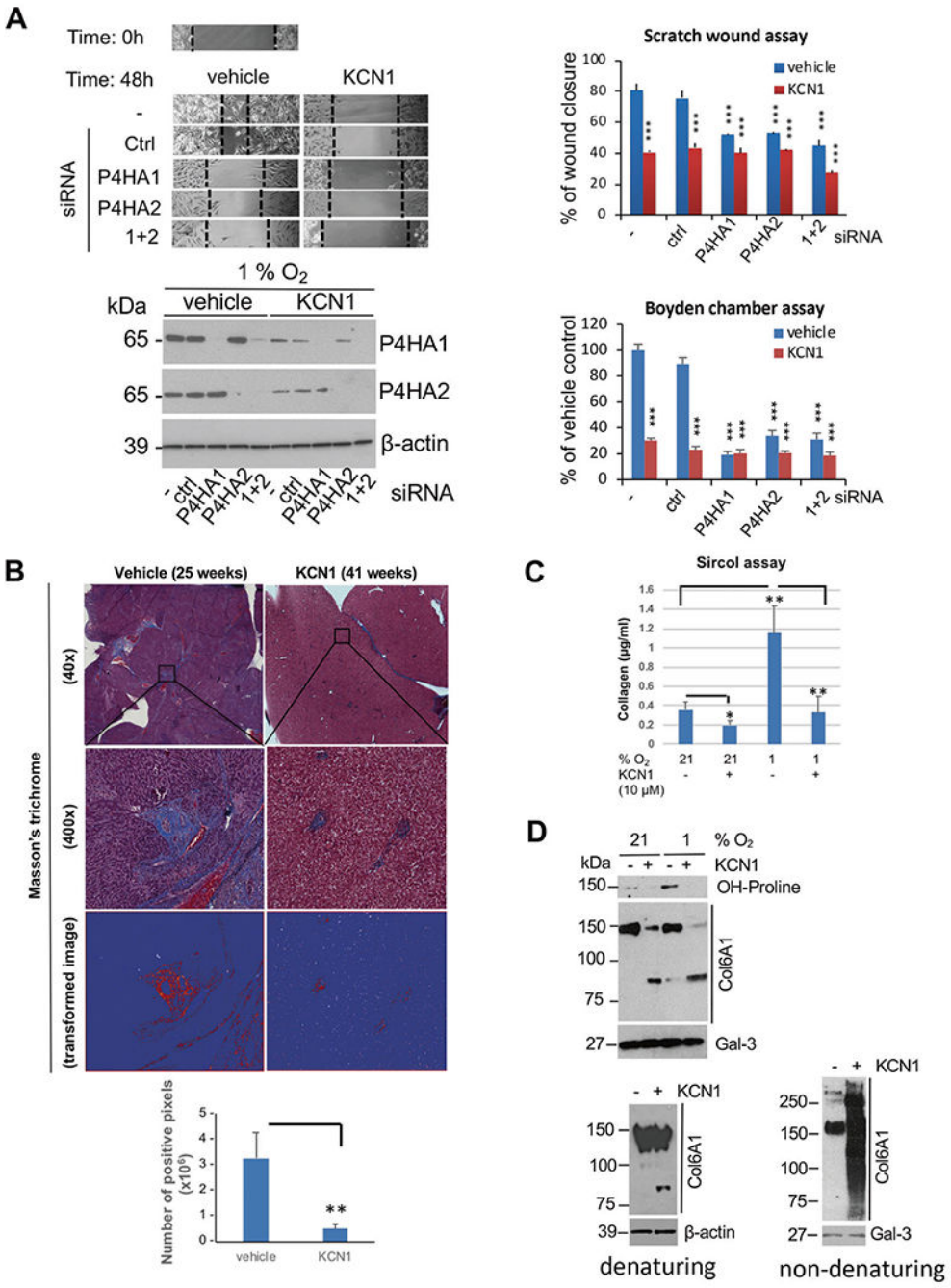

Fig. 4. Effect of KCN1 on hypoxia-induced collagen secretion and maturation by melanoma cells.

A Scratch wound migration and modified Boyden chamber Matrigel invasion assays show effect of RNAi-mediated silencing of P4HA1/2 expression ± KCN1 on hypoxia-induced UM cell motility. 92.1 cells were transfected with indicated siRNAs for 24 h, monolayers wounded, and cells incubated for an additional 48 h under hypoxic conditions. Top left, representative wound images. Top right, quantification of wound healing with Image J and expressed as percentage of wound closure in hypoxic control at the end of the experiment. ($n = 3$; ***$p < 0.001$ by two-tailed Student's t test). Bottom left, Western blot showing

efficacy of siRNA treatments. Bottom right, quantification of invaded cells expressed as percentage of invaded cells in hypoxic control at the end of the experiment. ($n = 3$; ***$p < 0.001$ by two-tailed Student's *t* test). **B** Masson's trichrome staining of mice livers (representative images; left) and quantitation (five fields; right) from the 92.1 experiment (Fig. 3). **$p < 0.01$ by two-tailed Student's *t* test. **C** Detection of soluble collagen in CM of B16LS9 cells collected at 24 h using a Sircol assay. Data are shown as means ± S.D. of triplicates, (*$p < 0.05$, **$p < 0.01$ by two-tailed Student's *t* test). Experiment was repeated twice independently ($N = 3$). **D** Analysis of secreted hydroxyproline-containing protein and collagen VI α1 chain by UM cells ± KCN1 treatment. Top, 92.1 UM cells were grown in serum-free medium ± KCN1 ± hypoxia (1% O_2) for 60 h, CM precipitated, 30 μg of protein analyzed by western blotting (7.5% gel) under denaturing conditions, and the membrane was sequentially probed with anti-hydroxyproline and anti-collagen VI α1 chain (Col6A1) antibodies. Gal-3 was used as a loading control. Bottom left, Western blot performed under denaturing conditions shows the presence of proteolytic product of α1(VI) in 92.1 tumor-bearing eyes From mice treated with vehicle (−) or KCN1 (+) from experiment in Fig. 3. Bottom right, detection of native collagen α1-containing collagen VI complexes in conditioned media from 92.1 cells by non-denaturing/non-reducing Western blot. Results were repeated three times independently ($n = 3$).